Synthesis, Structures, and Electrochemical Properties of Nickel Complexes of Macrocyclic N_2S_2 Aminothioethers

Ghezai Musie, Joseph H. Reibenspies, and Marcetta Y. Darensbourg*

Department of Chemistry, Texas A&M University, College Station, Texas 77843

Received May 8, 1997[⊗]

Macrocyclic complexes derived from the template synthesis of the *cis*-dithiolate nickel(II) complex [1,5-bis(mercaptoethyl)-1,5-diazacyclooctanato]nickel(II), **I**, and [*N*,*N*′-bis(2,2-dimethyl-2-mercaptoethyl)-1,5-diazacyclooctanato]nickel(II), **I***, with S to S linkers of C_2, **II***Br_2, C_3, **III***Br_2, and C_4, **IV***Br_2, were synthesized and fully characterized as square planar complex ions. The systematic enlargement of the N_2S_2 cavity size correlates with electrochemical measurements which find the $Ni^{II/I}$ couple to be more accessible through the series, while the Ni^{III} oxidation state is stabilized in the smaller cavities, maintaining an approximate 2 V difference between the $Ni^{III/II}$ and $Ni^{II/I}$ couples. The dithioether compound [**I***Me_2]I_2 shows the most positive $Ni^{II/I}$ potential (−412 mV vs NHE, in CH_3CN solution), consistent with the greater flexibility of the open-chain N_2S_2 ligand. While the reduced macrocycles show little tendency to react with carbon monoxide, EPR, electrochemical, and infrared spectroscopic studies of the Ni^{I} state of the open chain ligand complex support the reversible binding of CO in CO-saturated solutions. Cyclic voltammetry shows EC′ activity in the production of H_2 from HBF_4 solutions in the presence of the macrocycle complexes and is interpreted in terms of an inner-sphere Ni^{III}−H intermediate. Crystal data for **II***Br_2, **III***Br_2, and **IV***Br_2 are as follows: **II***$Br_2 \cdot {}^3/_2H_2O$ crystallizes in the monoclinic system, space group $P2_1/c$ with cell constants $a = 7.900(5)$Å, $b = 18.41(2)$ Å, $c = 15.612(14)$ Å, $\beta = 97.53(6)°$, $V = 2251(3)$ Å^3, and $Z = 4$, $R = 0.0972$, $R_w = 0.1886$; for **III***$Br_2 \cdot {}^5/_2H_2O$, monoclinic system, space group $P2_1/c$ with cell constants $a = 18.821(5)$ Å, $b = 7.844(2)$ Å, $c = 32.968(8)$ Å, $\beta = 97.84(2)°$, $V = 4824(2)$ Å^3, and Z = 8 and R = 0.077, $R_w = 0.125$; for **IV***$Br_2 \cdot H_2O$, orthorhombic system, space group *Pnma* with cell constants $a = 18.562(3)$ Å, $b = 15.140(3)$ Å, $c = 9.703(3)$ Å, V = 2726.8(11) Å^3, and $Z = 4$ and $R = 0.044$, $R_w = 0.099$.

Introduction

Several complexes containing nickel in lower oxidation states (Ni^0 and Ni^I) have been structurally characterized. Thus far, nickel(0) has been observed in soft, flexible donor environments (e.g. phosphines, thioethers, and carbonyls), approaching tetrahedral geometry in all.[1] In contrast, nickel(I) complexes have been isolated and crystallographically characterized with similar ligand sets, as well as the hard donor environment of tetraaza derivatives as shown in Scheme 1.[2−4] The flexible four-coordinate phosphino−thioether ligand defines a distorted square plane for Ni^{II} but is pseudo-tetrahedral in the Ni^0 complex, Scheme 1.[1] The distortion toward tetrahedral also prevails in the molecular structure of $[Ni^I(PMe_3)_4]^+$.[5] The pentacoordinate P_2S_2N ligand which defines a square pyramidal geometry for Ni^{II} distorts and expands toward a trigonal bipyramid for Ni^I.[3] In contrast, the square planar, N_4 cyclam complex undergoes minimal changes in geometry on reduction of Ni^{II} to Ni^I, only expanding the Ni−N distance by 0.12 Å.[4,6] Thus, the interpretation of the redox properties of these complexes must account for the metal−ligand acceptor−donor bond changes as well as geometrical transformations.[7]

Scheme 1

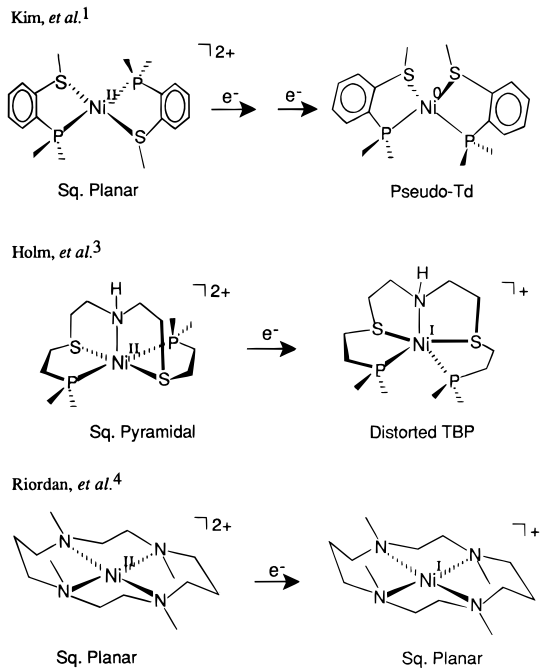

Although no study of the reactivity of the $[Ni^I(PMe_3)_4]^+$ complex has been reported,[5] it was recently shown that *stoichiometric* protonation of the $Ni^0P_2S_2$ complex of Scheme 1 leads to formation of Ni^{II}−H with no side evolution of hydrogen.[1] An $Ni^IP_2S_2N$ complex of Holm et al. has been shown to oxidize to Ni^{II} along with the release of a stoichiometric amount of H_2 in acidic (HCl) solutions.[3] The in depth

[⊗] Abstract published in *Advance ACS Abstracts,* December 15, 1997.

(1) Kim, J. S.; Reibenspies, J. H.; Darensbourg, M. Y. *J. Am. Chem. Soc.* **1996**, *118*, 4115, and references cited therein.
(2) Suh, M. P. *Adv. Inorg. Chem.* **1997**, *44*, 93.
(3) James, T. L.; Cai, L.; Muetterties, M. C.; Holm, R. H. *Inorg. Chem.* **1996**, *35*, 4148.
(4) Ram, M. S.; Riordan, C. G.; Ostrander, R.; Rheingold, A. L. *Inorg. Chem.* **1995**, *34*, 5884.
(5) Gleizes, A.; Dartiguenave, Y.; Galy, J.; Klein, H. F. *J. Am. Chem. Soc.* **1977**, *99*, 5187.
(6) Freeman, G. M.; Barefield, E. K.; Van Derveer, D. G. *Inorg. Chem.* **1984**, *23*, 3092.

S0020-1669(97)00526-0 CCC: $15.00
Published on Web 01/01/1998

Scheme 2

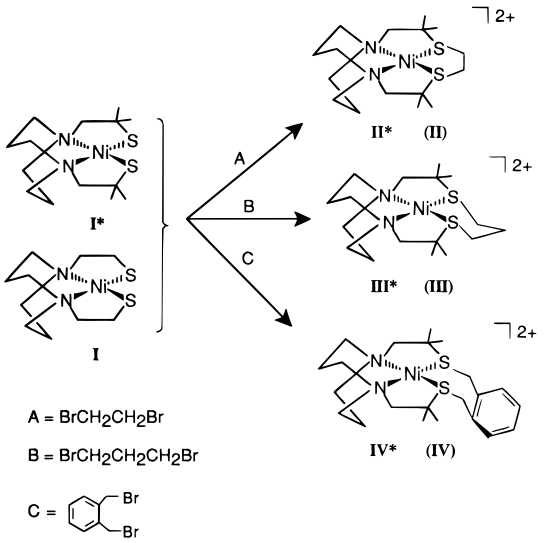

kinetic analysis of this dihydrogen-evolving reaction suggested an inner-sphere mechanism involving H^+ oxidative addition, $Ni^{III}-H$ formation, and chloride binding.

Herein we report five new N_2S_2Ni macrocyclic complexes of 14-, 15-, and 16-membered rings, which were synthesized by use of the well-known template effect of *cis*-dithiolates,[8] Scheme 2. The macrocyles exhibit a range of oxidation states of $Ni^{I,II,III}$ and, possibly, Ni^0 depending on the macrocycle size. In view of the above discussion, it was of interest to relate the macrocycle ring size with the redox potentials and to study, particularly, the Ni^I complexes and their reactivity toward protons and CO.

The impetus for the study of nickel-mediated chemistry in sulfur and sulfur/nitrogen donor environments derives from the discovery of a redox active nickel in [NiFe]−hydrogenase[9] and CO−dehydrogenase,[10−12] with characteristic EPR signals for odd-oxidation states. Organometallic-type precedents for the possible involvement of Ni^I and/or Ni^0 as intermediates in the catalytic processes which might involve oxidative addition of protons or Me^+, generating Ni−H or $Ni-CH_3$, are available for nickel in phosphorus/sulfur coordination.[1,13,14] The study below explores mononuclear nickel complexes in square planar N_2S_2 coordination, not as direct models of the active sites of [NiFe]−hydrogenase or CO−dehydrogenase (CO(DH)) which contain NiFe heterobimetallic units but rather for further understanding of factors which influence the accessibility of redox potentials and thermodynamic stabilities of different oxidation states. In the choice expression of Holm et al., with regard to abiological hydrogenase models, such studies are "first-generation experimental representation(s) of nickel-mediated dihydrogen evolution whose reactivity and mechanism indicate certain features obligatory to a functional analogue."[3]

Experimental Section

General Methods. Reagent grade solvents were dried and purified before use according to published procedures.[15] Specialty reagents were purchased from Aldrich Chemical Co. with the exception of $Ni(acac)_2$ (acac = acetylacetonate; Strem Chemical Co.) and used as received. Where anaerobic conditions were required, standard Schlenk techniques using argon (passed through a drying tube of $CaSO_4$, molecular sieves, and NaOH) and an argon-filled glovebox were employed. Elemental analyses were carried out by Galbraith Laboratories, Knoxville, TN.

Physical Measurements. UV−vis spectra were recorded on a Hewlett-Packard HP8452A diode array spectrophotometer. An IBM IR/32 Fourier transform spectrometer was used to record solution infrared spectra. Conductance measurements were performed using an Orion Model 160 conductance meter equipped with an Orion two-electrode conductivity cell manufactured by Sybron Corp. The cell constant was determined to be 0.112 cm^{-1}. Freshly distilled CH_3CN (distilled once from P_2O_5 and twice from CaH_2 under N_2) used in the conductivity measurements was found to have conductivity in the range of $(1.12-1.18) \times 10^{-6}\ \Omega^{-1}$.

EPR spectra were recorded on a Bruker ESP 300 equipped with an Oxford ER910A cryostat operating at 100 K. An NMR gaussmeter (Bruker Model ERO35M) and Hewlett-Packard frequency counter (Model HP5352B) were used to calibrate the field and microwave frequency, respectively. Samples, 0.15 mM in analyte, were frozen in liquid nitrogen prior to recording the EPR spectra. Reductants were cobaltocene, $NaBH_4$, and $KHB(sec\text{-}Bu)_3$. ^1H NMR spectra were obtained on a Varian XL200 spectrometer.

A BAS-100A electroanalyzer utilizing a three-electrode system with glassy carbon or Pt working electrode, platinum wire counter electrode, and a vycor-tipped $Ag/AgNO_3$ reference electrode was used for electrochemical measurements. Cyclic voltammograms were obtained from 2.5 mM analyte concentration in CH_3CN, using 0.1 M $[n\text{-}Bu_4N][PF_6]$ (TBAHFP) supporting electrolyte. Solutions were degassed by a purge of N_2 for 5 min, and a blanket of N_2 was maintained over the solution while the measurement was made. In the study for the calculation of CO binding, cyclic voltammograms were taken in a CO-saturated solvent and 1 atm of CO. The *iR* compensation between the working and reference electrodes was accomplished by applying the positive feedback from the BAS-100A current follower. All potentials were scaled to NHE using ferrocene as internal standard (Cp_2Fe^+/Cp_2Fe literature value is $E_{1/2}$(NHE) = 400 mV in acetonitrile).[16]

X-ray Crystallographic Determinations. The X-ray crystal structures were solved at the Crystal & Molecular Structure Laboratory Center for Chemical Characterization and Analysis at Texas A&M University. X-ray crystallographic data were obtained on a Siemens R3m/V single crystal X-ray diffractometer operating at 55 kV and 30 mA, M*o* Kα ($\lambda = 0.710\ 73$ Å) radiation equipped with a Siemens LT-2 cryostat. Several crystals of **II***Br_2 were examined. All of the crystals were small and poorly scattered X-rays. A marginal crystal was mounted on a glass fiber at room temperature and used for the experiment.

Preliminary examination and data collection for all crystals were performed on a Rigaku AFC5 (oriented graphite monochromator; Mo Kα radiation) at 163(2) K. Cell parameters were calculated from the least-squares fitting for 25 high-angle reflections ($2\theta > 15°$) for all experiments. ω scans for several intense reflections indicated very poor crystal quality for **II***Br_2 and acceptable quality for the remaining compounds. Data were collected for 5−45° at 163(2) K for **II***Br_2 and 5−50° on 2θ at 297(2) K for the remaining data sets. The scan width for data collection was $1.85 + 0.3 \tan\theta$, $1.56 + 0.03 \tan\theta$, and $1.45 + 0.3 \tan\theta$ in ω for **II***Br_2, **III***Br_2, **IV***Br_2 with a fixed scan rate of 8°/min for all data sets. Weak reflections were rescanned (maximum of two rescans), and the counts for each scan were accumulated.

For all data sets, three standards were collected every 197 reflections and showed no significant trends. Background measurement was by

(7) Geiger, W. E. *Prog. Inorg. Chem.* **1985**, *33*, 275.
(8) Thompson, M. C.; Busch, D. H. *J. Am. Chem. Soc.* **1964**, *86*, 3651.
(9) Boham, D.; Ludden, P. W. *J. Biol. Chem.* **1987**, *262*, 2980.
(10) Cramer, S. P.; Eidsness, M. K.; Pan, W.-H.; Morton T. A.; Ragsdale, S. W.; DerVartanian, D. V.; Ljungdahl, L. G.; Scott, R. A. *Inorg. Chem.* **1987**, *26*, 2477.
(11) Lindahl, P. A.; Kojima, N.; Hausinger, R. P.; Fox, J. A.; Teo, B. K.; Walsh, C. T.; Orme-Johnson, W. H. *J. Am. Chem. Soc.* **1984**, *106*, 3062.
(12) Scott, R. A.; Wallin, S. A.; Czechowski, M.; DerVartanian, D. V.; LeGall, J.; Peck, H. D., Jr.; Moura, I. *J. Am. Chem. Soc.* **1984**, *106*, 6864.
(13) Fisher, B.; Eisenberg, R. *J. Am. Chem. Soc.* **1980**, *102*, 7361.
(14) Meshitsuka, S.; Ichikwa, M.; Tamaru, K. *Chem. Commun.* **1974**, 158.
(15) Gordon, A. J.; Ford, R. A. *The Chemist's Companion;* Wiley: New York, 1972; pp 429−436.
(16) Gagne, R. R.; Koval, C. A.; Lisensky, G. C. *Inorg. Chem.* **1980**, *19*, 2854.

Table 1. Experimental Data for the X-ray Crystal Structures of **II***, **III***, and **IV***

	II*Br_2	**III***Br_2	**IV***Br_2
chem formula	$C_{16}H_{32}Br_2N_2S_2O_{1.5}Ni$	$C_{17}H_{39}Br_2N_2S_2O_{2.5}Ni$	$C_{24}H_{41}Br_2N_2S_2ONi$
fw	559.1	594.2	670.2
space group	monoclinic, $P2_1/c$	monoclinic, $P2_1/c$	orthorhombic, *Pnma*
a, Å	7.900(5)	18.821(5)	18.562(3)
b, Å	18.41(2)	7.848(2)	15.140(3)
c, Å	15.612(14)	32.968(8)	9.703(3)
β, deg	97.53(6)	97.84(2)	
V, Å^3	2251(3)	4824(2)	2726.8(11)
Z	4	8	4
ρ(calc), g/cm^3	1.660	1.636	1.633
temp, °C	−110	20	20
radiation (λ, Å)	Mo Kα (0.710 73)	Mo Kα (0.710 73)	Mo Kα (0.710 73)
abs coeff, mm^{-1}	4.608	4.307	3.818
abs correction type	Difabs	ψ-scan	ψ-scan
$R(F)$ $[I \geq 2\sigma(I)]$,[a] %	9.76	7.71	4.37
$R_w(F^2)$ $[I \geq 2\sigma(I)]$,[a] %	18.86	12.47	9.87

[a] Residuals: $R(F) = \sum|F_o - F_c|/\sum F_o$; $R_w(F^2) = \{[\sum w(F_o^2 - F_c^2)^2]/[\sum w(F_o^4)^2]\}^{1/2}$.

stationary crystal and stationary counter technique at the beginning and the end of each scan for half the total scan time. Lorentz and polarization corrections were applied to 3815 reflections for **II***Br_2, 8773 reflections for **III***Br_2, and 2511 reflections for **IV***Br_2. The empirical absorption correction DIF ABS was applied to **II***Br_2.[17] A semiempirical absorption correction was applied to **III***Br_2 and **IV***Br_2. All structures were solved by Direct Methods.[18a] Full-matrix least-squares anisotropic refinement of Ni, Br, S, and O and isotropic refinement of C and N on F^2 yielded $R(F)$ $[I > 2\sigma(I)] = 0.097$ and $R_w(F^2)$ $[I > 2\sigma(I)] = 0.1886$ at convergence for **II***Br_2.[18b] Full-matrix least-squares anisotropic refinement on all non-hydrogen atoms for **III***Br_2 and **IV***Br_2 yielded $R(F)$ $[I > 2\sigma(I)] = 0.077$ and $R_w(F^2)$ $[I > 2\sigma(I)] = 0.124$ for **III***Br_2 and $R(F)$ $[I > 2\sigma(I)] = 0.043$ and $R_w(F^2)$ $[I > 2\sigma(I)] = 0.098$. Hydrogen atoms are placed in idealized positions with isotropic thermal parameters fixed at 0.08 Å. Neutral atom scattering factors and anomalous scattering factors were taken from the International Table for X-ray Crystallography Vol. C. Cell parameter and data collection summaries for bromide complexes of **II***, **III***, and **IV*** are given in Table 1.

Syntheses. The syntheses of **I**,[19] **I***,[20] (3,3,11,11-tetramethyl-7-oxa-4,10-dithia-1,13-diazabicyclo[11.3.3]nonadecane)nickel(II) diiodide, **V***I_2,[20] (7-oxa-4,10-dithia-1,13-diazabicyclo[11.3.3]nonadecane)nickel-(II) diiodide, **V**I_2,[21] (4,8-dithia-1,11-diazabicyclo[9.3.3]heptadecane)-nickel(II) dibromide, **III**Br_2,[21] [*N*,*N*′-bis(3-thiabutyl)-1,5-diazacyclooctane]-nickel(II) iodide, [**I**Me_2]I_2,[21] and [*S*,*S*′-dimethyl-*N*,*N*′-bis(2-mercapto-2-methylpropane)-1,5-diazacyclooctane]nickel(II) iodide, [**I***Me_2]I_2[22] have been described elsewhere.

(4,7-Dithia-1,10-diazabicyclo[8.3.3]hexadecane)nickel(II) Dibromide, [(bme-daco)Ni$^{II}C_2H_4$]Br_2, IIBr$_2$. A 0.20 g (0.68 mmol) portion of **I** was dissolved in 15 mL of dichloromethane in a 50 mL round-bottomed flask. A 0.6 mL (7 mmol) portion of 1,2-dibromoethane was added; the flask was sealed, stirred for 2 h at 40 °C, and allowed to stand overnight. The solution turned red in ca. 10 min, and a portion of the product precipitated overnight. The solid product was isolated by filtration and redissolved in 1:1 (acetonitrile−methanol) and crystallized by diethyl ether diffusion into the solution, yielding 0.28 g (85%) of the product. The resulting dark red crystals were not suitable for X-ray diffraction studies. A cocrystallized water molecule is included in the calculated elemental analysis. Anal. Calcd (found) for $NiS_2N_2C_{12}H_{26}Br_2.H_2O$: C, 29.89 (28.74); H, 5.28 (5.27); N, 5.56 (5.61).

(6,7-Phenyl-4,9-dithia-1,12-diazabicyclo[10.3.3]octadecane)nickel-(II) Dibromide, [(bme-daco)Ni$^{II}CH_2C_6H_4CH_2$]Br_2, IVBr$_2$. In a manner similar to that above, 0.23 g of α,α′-dibromo-*o*-xylene that was dissolved in 10 mL of methanol was transferred by cannula into a 50 mL round-bottomed flask containing a purple solution of **I** (0.30 g, 1.02 mmol) in 20 mL of acetonitrile. After the solution was stirred at 40 °C for 2 h, its color shifted to green. On standing the reaction mixture overnight, a green solid fell out of the solution and was collected by filtration. A portion of the solid product was recrystallized from slow diffusion of ether into the methylene chloride solution of the green product. The resulting green crystals were collected by filtration and dried in air with a yield of 0.40 g (93% based on **I**). Anal. Calcd (found) for $NiS_2N_2C_{18}H_{28}Br_2$: C, 38.9 (37.2); H, 5.08 (5.26); N, 5.05 (5.01).

(3,3,8,8-Tetramethyl-4,7-dithia-1,10-diazabicyclo[8.3.3]hexadecane)-nickel(II) Dibromide, [(bme*-daco)Ni$^{II}C_2H_4$]Br_2, II*Br$_2$. In a similar manner a purple acetonitrile solution (15 mL) of **I*** (0.25 g, 0.72 mmol) was added to a dichloromethane solution containing 1,2-dibromoethane (0.6 mL, 7 mmol). The resulting solution was stirred at 40 °C for ca. 30 min, until the color became dark red, and left undisturbed at room temperature. Overnight a red solid product was obtained, from which the mother liquor was decanted; after washing with ether, the yield was 0.28 g (72% based on **I***). Crystals suitable for single crystal X-ray analysis were obtained by ether diffusion into a methanol−acetonitrile(1:1) solution of the product. Anal. Calcd (found) for $NiS_2N_2C_{16}H_{32}Br_2.0.5H_2O$: C, 34.3 (33.9); H, 5.90 (6.00); N, 5.01 (4.89).

(3,3,9,9-Tetramethyl-4,8-dithia-1,11-diazabicyclo[9.3.3]hep-tadecane)nickel(II) Dibromide, [(bme*-daco)Ni$^{II}C_3H_6$]Br_2, III*Br$_2$. A 0.30 g (0.86 mmol) portion of **I*** was dissolved in 20 mL of methylene chloride in a 50 mL Erlenmeyer flask, and 1.2 mL (12 mmol) of 1,3-dibromopropane was added in one portion. After a brief mixing of the reaction mixture, the flask was stoppered and allowed to stand undisturbed for 24 h. The solution turned deep orange in color, and orange crystals settled out overnight. The mother liquor was decanted from the solid product, which after drying weighed 0.3 g. Treating of the orange-colored mother liquor with diethyl ether gave a further 0.07 g of product for a total yield of 78% based on **I***. X-ray quality crystals formulated as $C_{17}H_{34}N_2S_2Br_2Ni\cdot2.5H_2O$ were obtained from ether diffusion into a solution of the orange product in dichloromethane−acetonitrile (1:1). Anal. Calcd (found) for $C_{17}H_{34}N_2S_2Br_2Ni\cdot2.5H_2O$: C, 34.3 (34.1); H, 6.60 (6.10); N, 4.72 (4.56).

(3,3,10,10-Tetramethyl-6,7-phenyl-4,9-dithia-1,12-diazabicyclo-[10.3.3]octadecane)nickel(II) Dibromide, [(bme*-daco)Ni$^{II}CH_2C_6$-H_4CH_2]Br_2, IV*Br$_2$. A yellow solution of α,α′-dibromo-*o*-xylene in methanol (0.23 g, 10 mL) was added to an orange solution of **I*** (0.3 g, 0.86 mmol) in 20 mL of acetonitrile. The resulting green solution was stirred at 40 °C for 4 h and left overnight at room temperature. The solvent was evaporated by vacuum. The crude product was

(17) Walker, N.; Straurt, D. *Acta. Crystallogr.* **1983**, *A39*, 158.
(18) (a) Sheldrick, G. *SHELXTL-86, Program for Crystal Structure Solution*; Institüt für Anorganische Chemie der Universität: Gottingen, Germany, 1986. (b) Sheldrick, G. *SHELXTL-93, Program for Crystal Structure Solution*; Institüt für Anorganische Chemie der Universität: Gottingen, Germany, 1993.
(19) Mills, D. K.; Reibenspies, J. H.; Darensbourg, M. Y. *Inorg. Chem.* **1990**, *29*, 4364.
(20) Darensbourg, M. Y.; Font, I.; Pala, M.; Reibenspies, J. H. *J. Coord. Chem.* **1994**, *32*, 39.
(21) Darensbourg, M. Y.; Font, I.; Mills, D. K.; Pala, M.; Reibenspies, J. H. *Inorg. Chem.* **1992**, *31*, 4965.
(22) Font, I. Ph.D. Dissertation, Texas A&M University, College Station, TX, 1994.

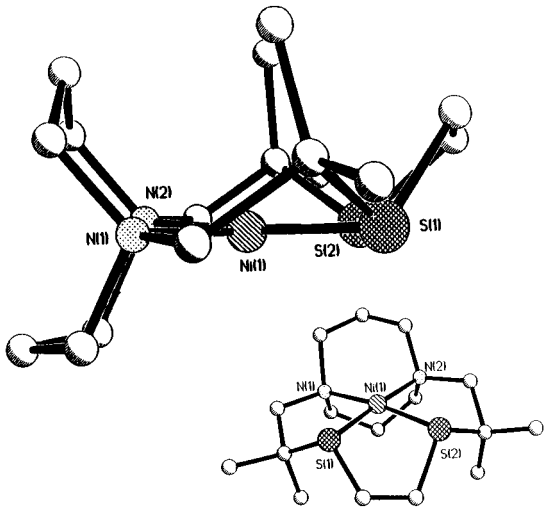

Figure 1. Molecular structure of $C_{16}H_{32}Br_2N_2S_2Ni$, **II***Br_2, with numbering scheme and alternate view. Hydrogen atoms and water(s) of crystallization are omitted. Selected bond lengths (Å): Ni(1)−N(1), 1.94(2); Ni(1)−N(2), 1.97(2); Ni(1)−S(1), 2.154(9); Ni(1)−S(2), 2.167(9). Selected bond angles(deg): N(1)−Ni(1)−N(2), 92.4(2); N(1)−Ni(1)−S(1), 90.2(7); N(2)−Ni(1)−S(1), 177.0(7); N(1)−Ni(1)−S(2), 173.5(7); N(2)−Ni(1)−S(2), 91.5(7); S(2)−Ni(1)−S(1), 85.8(3).

recrystallized from methylene chloride and diethyl ether. The resulting dark red crystals, formulated as $NiS_2N_2C_{22}H_{36}Br_2 \cdot 2H_2O$ and suitable for X-ray analysis, were collected by filtration and dried in air with a yield of 0.40 g (76% based on **I***). Anal. Calcd (found) for $NiS_2N_2C_{22}H_{40}O_2Br_2$: C, 40.8 (41.1); H, 6.2 (6.2).

IR Sample Preparation. To a 123 mg (0.22 mmol) portion of iodide salt of [**I**Me_2] dissolved in 10 mL of thoroughly degassed and dry acetonitrile was added anaerobically 8 mg (0.24 mmol) of $NaBH_4$, dissolved in 10 mL of acetonitrile. A color change from green to light yellow was noticed. This yellow solution turned light green when purged with carbon monoxide and kept under CO. A portion of the light green solution was rapidly transferred by syringe into a standard CaF_2 IR cell with a 0.1 mm path length, and the spectrum was recorded. Low-temperature IR measurements were taken quickly after cold samples (immersed in a dry ice (CO_2)/ethylene glycol bath) of the reduced complex in the presence of CO were transferred into a cell (which was cooled on dry ice). In addition to $NaBH_4$, Na/Hg was also used as reductant with similar results.

Results and Discussion

The well-known template effect[8,23] exhibited by *cis*-thiolates in the nickel(II) complexes **I** and **I*** has led to efficient (80−90% isolated yields) syntheses of new N_2S_2 macrocyclic complexes. Thus, a series is available in which the S···S linker is derived from $\alpha-\omega$ bromocarbons and includes the range given in Scheme 2; for comparison the open chain, [**I***Me_2]I_2[22] will also be discussed. An earlier synthetic effort based on **I** provided the three carbon linked macrocycle **III**Br_2.[21] The use of $ICH_2CH_2OCH_2CH_2I$ produced a five-atom-linked, potentially pentadentate ligand, where derivative complex cations are represented as **V** and **V***.[20,21] Attempts to react **I** and **I*** with CH_2Br_2 and CH_2I_2 led to highly hygroscopic and unstable products. Complexes **II***Br_2, **III***Br_2, and **IV***Br_2 were obtained in crystalline forms and subjected to X-ray crystallographic analyses.

Crystal and Molecular Structures. The molecular structures of the cations of **II***Br_2, **III***Br_2, and **IV***Br_2 are shown in Figures 1−3, respectively; selected bond angles and bond lengths are given in the figure captions. In all macrocycle

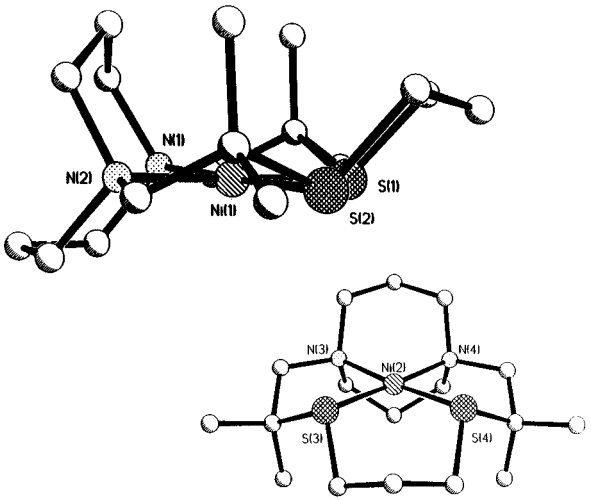

Figure 2. Molecular structure of $C_{17}H_{34}Br_2N_2S_2Ni$, **III***Br_2. Hydrogen atoms and water(s) of crystallization are omitted. Selected bond lengths (Å): Ni(1)−N(1), 1.972(8); Ni(1)−N(2), 1.983(8); Ni(1)−S(1), 2.177(3); Ni(1)−S(2), 2.176.(3); Ni(2)−N(3), 1.982(8); Ni(2)−N(4), 1.982(8); Ni(2)−S(3), 2.167(3); Ni(2)−S(4), 2.186(3). Selected bond angles(deg): N(1)−Ni(1)−N(2), 91.4(3); N(1)−Ni(1)−S(1), 88.4(2); N(2)−Ni(1)−S(1), 177.6(3); N(1)−Ni(1)−S(2), 177.2(3); N(2)−Ni(1)−S(2), 87.8(3); S(2)−Ni(1)−S(1), 92.3(12); N(3)−Ni(2)−N(4), 91.0(3); N(3)−Ni(2)−S(3), 87.7(2); N(4)−Ni(2)−S(3), 177.0(3); N(3)−Ni(2)−S(4), 174.8(3); N(4)−Ni(2)−S(4), 87.9(3); S(4)−Ni(2)−S(3), 93.08(11).

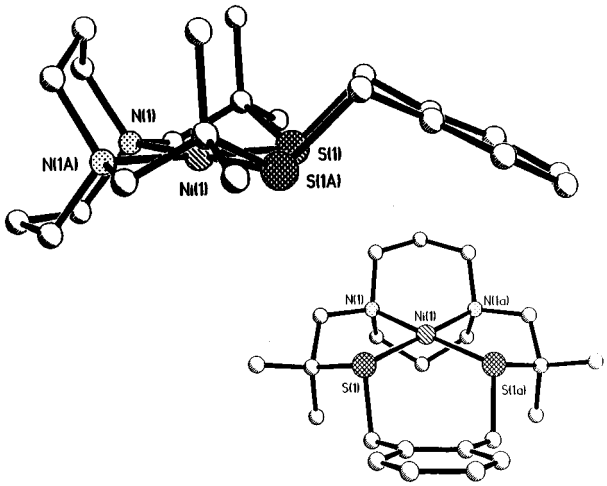

Figure 3. Molecular structure of $C_{24}H_{36}Br_2N_2S_2Ni$, **IV***Br_2. Hydrogen atoms and waters of crystallization are omitted. The atoms labeled a are related by a crystallographic center of symmetry. Selected bond lengths (Å): Ni(1)−N(1), 1.997(4); Ni(1)−N(1a), 1.997(4); Ni(1)−S(1), 2.2163(14); Ni(1)−S(1a), 2.2162(14). Selected bond angles(deg): N(1)−Ni(1)−N(1a), 89.8(3); N(1)−Ni(1)−S(1a), 177.77(14); N(1a)−Ni(1)−S(1a), 87.95(13); N(1)−Ni(1)−S(1), 87.95(13); N(1a)−Ni(1)−S(1), 177.77(14); S(1a)−Ni(1)−S(1), 94.28(7).

complexes the nickel is found in substantially square planar geometry, with average deviations of atoms from the best least-squares N_2NiS_2 plane no greater than 0.06 Å and typically around 0.03 Å. Tetrahedral twists defined as the dihedral angles of the N_2Ni and NiS_2 planes are 5.3, 3.7, and 5.9° for **II***$^{2+}$, **III***$^{2+}$, and **IV***$^{2+}$, respectively. Comparisons of interatomic distances and angles are given in Table 2.

The ethylene thiol arms of the ligands are eclipsed across the NiN_2S_2 plane in all complexes, with the methyl substituents on the carbons α to sulfurs in axial and equatorial positions. In all structures, the two fused nickel−diazacyclohexane metallacycles are in the chair/boat configuration with the boat form on the same side of the NiN_2S_2 plane as the axial methyl groups

(23) Rose, N. J.; Root, C. A.; Busch, D. H. *Inorg. Chem.* **1967**, *6*, 1431.

Table 2. Selected Interatomic Distances and Angles for Dithioether Derivatives of **I***

complex	av Ni−N, Å *Ni−S, Å*	S···S, Å	∠S−Ni−S, deg	∠Ni−S−C_{linker}, deg
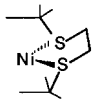	1.955(2) *2.161(9)*	2.942	85.8(3)	103.4 99.6
II*				
	1.976(8) *2.177(3)*	3.092	92.3(3)	112.8 113.8
III*				
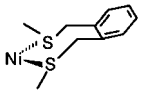	1.997(4) *2.216(4)*	3.249	94.3(7)	115 115
IV*				
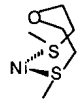	1.976(6)[a] *2.196(2)*[a]		87.7(1)	103.2 103.0
V*				
	*1.966(2)*[b] *2.173(1)*[b]	3.050	89.7(1)	103.6 111.6
$[I^*Me_2]^{2+}$				

[a] Data from ref 20, where **V*** is crystallized as a I^- salt. [b] Data from ref 22, where $[\mathbf{I}Me_2]^{2+}$ is crystallized as a $[BPh_4]^-$ salt.

of the ethylene thiol pendant arms. This configuration provides much steric blockage and is expected to inhibit axial coordination on one face of the complex. The two α carbons in the S to S spacers are also oriented in the same direction as the hydrocarbon-rich side of the square plane, resulting in the opposite face of the complex being quite open, exposing the sulfurs and the nickel. This plane is best seen in the alternate views of the complexes shown in Figures 1−3. The possibility of additional coordination on the open side is realized by the inclusion of a water molecule for $\mathbf{IV}^{*2+}$ at a distance of 2.58 Å, substantially longer than the typical Ni−OH_2 bond distance which ranges from 2.0 to 2.2 Å.[24]

For $\mathbf{II}^*Br_2$ the nonbonded atom closest (3.05 Å) to the nickel is an oxygen from a cocrystallized water molecule. As in $\mathbf{IV}^*Br_2$, the nickel oxygen vector is roughly perpendicular to the NiN_2S_2 plane and thus could also indicate a long-range axial ligand. As indicated in Table 2, between $\mathbf{II}^*Br_2$ and $\mathbf{IV}^*Br_2$ the average Ni−N and Ni−S bond lengths increase by 0.04 and 0.05 Å, respectively, the S(1)−Ni−S(2) bite angle increases significantly by 8.5°, and the S to S distance increases by ca. 0.31 Å. Since the coordination number of 4 throughout the complexes is maintained, these changes reflect the increase of cavity size of the ligand as the carbon chain of the S to S link increases. The Ni−S−C angles within the nickel−dithioether cycle vary within the series, showing the smallest values for $\mathbf{II}^{*2+}$, reflecting the greater rigidity of the smallest macrocycle.

The crystal structures of $\mathbf{V}^{2+}$ and $\mathbf{V}^{*2+}$ as their iodide salts have been previously determined.[20,21] Whereas the former demonstrates the propensity of hexacoordination to result from the induction of axial halide binding trans to the O-atom donor,[25] the steric hindrance of the hydrocarbon blocked face of the **V*** derivative prevents halide binding and, as a result, the O-atom of the ether linkage is beyond the bonding distance to nickel. The conformation of the $\overline{NiS(CH_2)_2O(CH_2)_2S}$ eight-membered ring is, however, boatlike and places the O-atom at the rather close distance of 2.43(5) Å. The bromide salts of $\mathbf{V}^{2+}$ and $\mathbf{V}^{*2+}$ are available through ion exchange reactions[20,21] and are used for comparisons below.

Solution Characterization. Earlier detailed studies of similar complexes in water and acetonitrile solvents concluded that the tetracoordinate, square planar N_2S_2 (S = thioether) nickel complexes commonly form orange to red solutions, whereas higher coordination numbers, or strong site specific ion pairing (anation), or site specific ligation by solvent produces green or blue solutions.[20,21] In the cases of the **I** and **I*** macrocycle derivatives, the colors and electronic spectroscopic data which are presented in Table 3 may be similarly interpreted as representative of either dicationic square planar $[N_2S_2Ni]^{2+}$ complexes, dicationic pentacoordinate $[N_2S_2Ni(Solv)]^{2+}$, monocationic pentacoordinate $[N_2S_2Ni(X)]^+$, or hexacoordinate $[N_2S_2Ni(X)(Solv)]^+$ complexes, respectively, involving ionic equilibria such as the following.

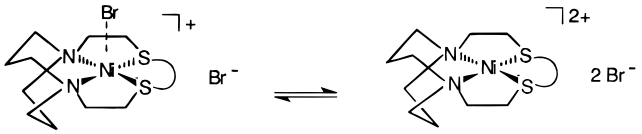

Since hexacoordination is not expected for the sterically hindered **I*** derivatives, the green colors of $\mathbf{IV}Br_2$ and $\mathbf{IV}^*Br_2$ in acetonitrile solution are ascribed to pentacoordinate species. Since the usual ranges of 2:1 and 1:1 electrolytes are 200−280 and 120−160 $cm^2\ \Omega^{-1}\ mol^{-1}$, respectively in acetonitrile,[26] we conclude from the molar conductance values in Table 3 that $\mathbf{IV}Br_2$ and $\mathbf{IV}^*Br_2$ are di-uni electrolytes and thus are solvated $[N_2S_2Ni(Solv)]^{2+}$, rather than $[N_2S_2Ni(Br)]^+$. Only complex $\mathbf{V}Br_2$ is in the uni-uni electrolyte category and as discussed earlier, suggests the ionic equilibrium is shifted toward hexacoordinate $[\mathbf{V}Br]^+$. It should be noted that the higher coordination numbers derived from either solvation or anation induces paramagnetism which could account for the broad peaks observed in the ^1H NMR spectra for the macrocyclic complexes. Nevertheless the peak positions are in the usual ranges as seen for the neutral parent dithiolate **I*** and its S−oxygenate derivatives.[27]

Electrochemical Properties. Cyclic voltammograms of complexes $\mathbf{II}^*Br_2$, $\mathbf{III}^*Br_2$, and $\mathbf{IV}^*Br_2$ are shown in Figure 4, and electrochemical data are given in Table 4. All potentials are referenced to NHE. Two reversible couples and one irreversible oxidation event are common features of all complexes with a bromide counter ion, whereas the tetrafluoroborate counterparts lack the irreversible oxidation peak at 750 mV. Thus, the irreversible wave is assigned to the oxidation of bromide to bromine. Further scanning toward more positive potential gave quasi reversible waves in the 1100−1200 mV

(24) Orpen, A. G.; Brammer, L.; Allen, F. H.; Kinnard, O.; Watson, D. G.; Taylor, R. *J. Chem. Soc., Dalton Trans.* **1989**, S1.

(25) Goodman, D. C.; Farmer, P. J.; Darensbourg, M. Y.; Reibenspies, J. H. *Inorg. Chem.* **1996**, *35*, 4989.

(26) Greary, W. *J. Coord. Chem. Rev.* **1971**, *7*, 81.

(27) (a) Buonomo, R. M.; Font, I.; Maguire, M. J.; Reibenspies, J. H.; Tuntulani, T.; Darensbourg, M. Y. *J. Am. Chem. Soc.* **1995**, *117*, 963. (b) Darensbourg, M. Y.; Tuntulani, T.; Reibenspies, J. H. *Inorg. Chem.* **1995**, *34*, 6287.

Table 3. Characterization of the Bromide and Iodide Salts of N_2S_2Ni Macrocycles

complex	color solid/H_2O/CH_3CN	Λ_M,[a] cm^2 Ω^{-1} mol^{-1}	λ, nm (ϵ, M^{-1} cm^{-1}) water	λ, nm (ϵ, M^{-1} cm^{-1}) acetonitrile
IIBr_2	black/red/red	266	410 (169), 488 (174)	410, 488 (154)
II*Br_2	brown/yellow/yellow	211	458 (213)	460 (206)
IIIBr_2	purple/red/violet	218	484 (287)	410 (151), 581 (142)
III*Br_2	orange/yellow/orange	206	454 (133)	464 (180)
IVBr_2	green/pink/green	249	404 (124), 590 (110)	422 (120), 620 (118)
IV*Br_2	red/red/green	231	480 (179)	422 (158)
VI[21]	green/pink/green	138	470 (166)	417 (171), 640 (67)
V*I_2[20]	brown/brown/green		465 (102), 584 (98)	460 (112), 384 (132)
[**I**Me_2]I_2[21]	green/coral/yellow		408 (165), 486 (102)	410 (160), 490 (98)
[**I***Me_2]I_2[22]	orange/yellow/yellow	205	470 (165)	466 (115)

[a] Molar conductance values for ca. 1 mM solutions in CH_3CN.

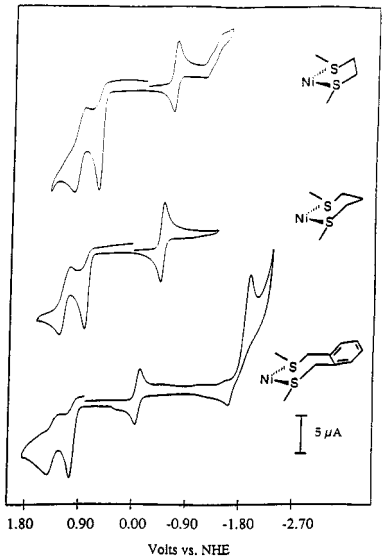

Figure 4. Cyclic voltammograms of 2.5 mM solutions of (a, top) **II***Br_2, (b, middle) **III***Br_2, and (c, bottom) **IV***Br_2 in 0.1 M TBAHFP/CH_3CN with a glassy carbon working electrode at a scan rate of 150 mV/s. All potentials are scaled to NHE using Cp_2Fe^+/Cp_2Fe as internal standard ($E_{1/2}$ = 0.40 mV).[16] [Note: The *x* axis scale is compressed for c.]

Table 4. Electrochemical and Reversibility Data of the Complexes from Cyclic Voltammetry in CH_3CN Solutions[a]

complex	$Ni^{III/II}$ $E_{1/2}$, mV	ΔE_p	$i_{pc/ipa}$	$Ni^{II/I}$ $E_{1/2}$, mV	ΔE_p	$i_{pc/ipa}$	$Ni^{I/0}$ E_{pc}, mV
IIBr_2	1123	172	0.83	−781	61	0.97	
IIIBr_2	1160	146	0.91	−670	63	1.03	
IVBr_2	1235	128	0.70	−523	60	1.01	−2156
II*Br_2	1146	164	0.73	−761	64	1.01	
III*Br_2	1167	187	0.82	−591	65	0.98	
IV*Br_2	1265	146	0.80	−432	60	1.01	−2284
VI[21]				−630	140	0.53	
V*$I_2$20				−453	80	0.90	
[**I**Me_2]I_2	1568	76	0.97	−482	72	0.98	
[**I***Me_2]I_2	1578	112	0.88	−412	65	0.99	

[a] In solutions of CH_3CN and 0.1 M tetrabutylammonium hexafluorophosphate (TBAHFP) supporting electrolyte; scan rate of 200 mV/s. All entries referenced to NHE using Cp_2Fe^+/Cp_2Fe ($E_{1/2}$ = 400 mV) as internal standard.

range that are assigned to $Ni^{III/II}$ couples. The reversible waves at negative potentials are assigned to $Ni^{II/I}$ couples (for example, the reversible reduction wave at −591 mV for **III***Br_2), and this assignment is confirmed by EPR studies on chemically reduced complexes as described below. The values of ΔE_p and peak current ratios for $Ni^{II/I}$ are consistent with one electron transfer processes. The $Ni^{II/I}$ redox processes are uncoupled with any chemical reaction as the $E_{1/2}$ values are constant with different scan rates (50−750 mV/s).

Figure 4c shows the electrochemical response of complex **IV***Br_2. The reversible reduction wave at −432 mV is assigned to the $Ni^{II/I}$ couple. Further scanning toward more negative potential indicated an irreversible (or quasi reversible) reduction at −2.28 V at the edge of the CH_3CN solvent potential window. (A similar feature was also observed for complex **IV**Br_2 at −2.15 V. In addition, the CH_3CN solution cyclic voltammogram of **IV**Br_2 has waves at −523 mV and 1.24 V, which are assigned to $Ni^{II/I}$ and $Ni^{III/II}$, respectively.) Since the cyclic voltammograms of the free ligands (obtained by the displacement of the nickel by KCN in aqueous solution followed by ether extraction of the free ligand) show no electrochemical activity within the solvent potential window, it is reasonable that the events are due to $Ni^{I/0}$ reduction. Alternatively, as suggested by a reviewer, the large current peak of the most negative wave may be indicative of a ligand-based, i.e., aromatic ring reduction, consistent with the known faster electron transfer rates in organic molecules. If such were the case, it would also imply a substantial shift in aromatic ring potential on binding to the metal. Importantly, the $Ni^{I/0}$ couples of phosphino−thioether complexes of the bidentate ligand shown in Scheme 1, as well as the similar open chain phosphino−thioether complexes of nickel, are fully reversible and more positive by ca. 1400−1500 mV.[1] Thus, the irreversibility of the (assumed) $Ni^{I/0}$ in the N_2S_2 macrocycles is attributed to the structural rigidity of the complexes, which prevents the distortion toward tetrahedral upon reduction, as well as the orbital mismatch of the hard tertiary nitrogen donor sites of the daco framework to the soft Ni^0.

The data given in Table 4 indicate a dependence of $E_{1/2}$ on the overall ligand ring size, ligand flexibility, and S-donor character. Within the series **II***Br_2 to **IV***Br_2 a gain of 329 mV for the $Ni^{II/I}$ couple is realized. The same trend, toward more positive potentials, is observed for the $Ni^{III/II}$ couple. The maximum stabilization of Ni^I is attained with the more flexible open-chain ligands, [**I**Me_2]$^{2+}$ and [**I***Me_2]$^{2+}$, followed by the largest macrocycles **IV**Br_2 and **IV***Br_2. Figure 5 shows that the correlation of the S to S atom links with $E_{1/2}$ values of the $Ni^{II/I}$ potentials for both the **I** and **I*** macrocyclic series is linear for 2- to 4-atom links. Complexes **V**Br_2 and **V***I_2, the N_2S_2O macrocycles, which show a tendency for O-atom binding in the crystal structures, clearly lie off their respective lines with less accessible $Ni^{II/I}$ potentials. Importantly, **V*I$_2$** is more closely placed to the correlation than is **V**Br_2; the latter is undoubtedly a penta- or hexacoordinate complex in solution. The steric hindrance of the former inhibits the axial binding.

The macrocycle derivatives of **I** show more accessible Ni^{III} in comparison to those of **I***, e.g., **II**Br_2 vs **II***Br_2, Table 4.

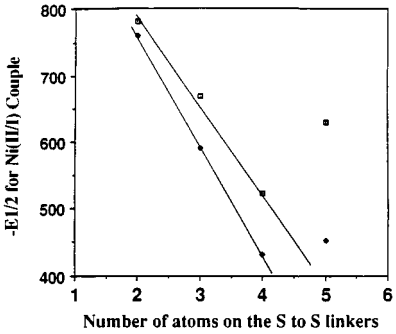

Figure 5. Correlation of the number of S to S atom links with the $E_{1/2}$ value of the $Ni^{II/I}$ potentials for both **I** (⊡) and **I*** (●) macrocycle series.

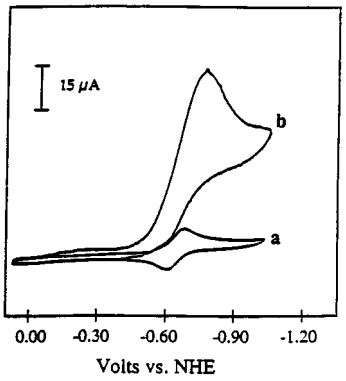

Figure 6. Cyclic voltammograms of DMF solutions (a) of **III***Br_2 and (b) in the presence of 10 equiv of HBF_4 using a platinum working electrode. Experimental conditions are the same as in the caption of Figure 4.

This result is consistent with the steric hindrance of the methyl groups α to S in the latter which prevents solvent interaction with the metal center. The expansion of the coordination number that is associated with the formation of Ni^{III} is completed by the solvent axial ligation; hence, the less sterically hindered macrocycles derivative of **I** are superior in stabilizing Ni^{III}. A similar observation was noted in the case of cyclam vs the methylated cyclam nickel complexes.[28]

Stability of the Ni^{II} and Ni^{I} Complexes toward Acid. The stability of the Ni^{II} complexes toward HCl and HBF_4 acids, even in 1 M HCl/water, HCl/acetonitrile, and HCl/DMF, was indicated by the fact that the UV−vis spectra of the complexes are the same as those in neutral pH solutions. Cyclic voltammograms obtained for complexes **III**Br_2 and **III***Br_2 at various potential scan rates at glassy carbon and platinum electrodes in *N*,*N*′-dimethylformamide, DMF, show $Ni^{II/I}$ redox couples similar to those reported above for the acetonitrile solutions. Further electrochemical activity was not observed upon scanning to more negative potentials within the range of the medium. However, the presence of HBF_4 in the DMF solution brought the change in the voltammogram shown in Figure 6. The $Ni^{II/I}$ couple of **III***Br_2 becomes completely irreversible, the reduction peak increases in current, and the oxidation peak decreases, as is typical of reduction followed by a rapid chemical reaction that regenerates the reactant, in this case Ni^{II}. The ratio of the cathodic peak current to the square root of the scan rate increases greatly (by 260%) upon decreasing the scan rate by 4-fold. Such behavior is typical of an EC′ mechanism, electron transfer followed by a rapid chemical reaction(s) that regenerate(s) the oxidized species.[29]

Scheme 3

$$Ni^{II} + e^- \rightleftharpoons Ni^{I}$$

$$Ni^{I} + H^+ \longrightarrow Ni^{III}\text{-}H$$

(a) $$Ni^{III}\text{-}H + H^+ \longrightarrow Ni^{III} + H_2$$

$$Ni^{III} + e^- \rightleftharpoons Ni^{II}$$

(b) $$2\,Ni^{III}\text{-}H \longrightarrow 2\,Ni^{II} + H_2$$

(c) $$Ni^{III}\text{-}H + e^- \rightleftharpoons Ni^{II}\text{-}H$$

$$Ni^{II}\text{-}H + H^+ \longrightarrow Ni^{II} + H_2$$

The electrolysis potential value at 99% completion may be calculated from the Nernst equation, $E = E^{\circ\prime} + RT/nF \ln\{(C_o(t)/C_r(t)\}$; at 99% completion $C_o(t) = 1$, $C_r(t) = 99$, and $E = E^{\circ\prime}$ - 118 mV. Thus, in the presence of HBF_4, reductive electrolysis at −804 mV (that is, −686 mV, the $Ni^{II/I}$ reduction couple of III in DMF minus 118 mV) for **III**Br_2 and −726 mV (−608 to +118 mV) for **III***Br_2 was applied until the current ratio dropped by 99%. Production of hydrogen gas was witnessed at the surface of the electrodes, the platinum being more efficient than the glassy carbon. A shorter electrolysis time was observed for the **III***Br_2 complex and indicated a greater catalytic efficiency than **III**Br_2 under the same experimental conditions. After exhaustive electrolysis the product solutions showed higher pH values, indicative of the reduction of hydrogen ions, but an identical electrochemical response, in pattern and in the size of peak current, as observed for the **III**Br_2 and **III***Br_2 pure compounds prior to the addition of acid and electrolysis. This suggests that the complexes are stable throughout the catalytic process.

Thermodynamic free energy calculations by Parker have found the standard reduction potential value of H^+ to be −2.35 V vs NHE in CH_3CN solvent;[30] thus, its reduction at −0.60 V by the Ni^{I} species indicates a distinct catalytic function of the complex. Such a gain of more than 1 V in the reduction of H^+ is typically attributed to an inner-sphere process.[31] In this case presumably the Ni^{I} is protonated, producing a transient Ni^{III}−H, which on subsequent protonation (mechanism a of Scheme 3) or loss of $H^{\bullet}$ (mechanism b of Scheme 3) produces H_2. A third possibility is an ECEC mechanism, where the reduction of Ni^{III}−H is more accessible than Ni^{II}. In that case the resulting Ni^{II}−H intermediate will be protonated to produce H_2 and Ni^{II} (mechanism c of Scheme 3). These schemes are similar to those proposed by Holm et al., in explanation of the nickel-mediated production of H_2 observed for the pentacoordinate Ni(I) complex of the P_2S_2N donor set (shown in Scheme 1).[3]

Bulk Chemical Reduction and Protonation. The addition of 1 equiv of cobaltocene to acetonitrile solutions of **III***Br_2 resulted in a change of color, from orange to dark green. On immediate addition of HBF_4, evolution of gas was observed. Under identical conditions excepting the absence of **III**Br_2 or **III***Br_2, addition of HBF_4 to Cp_2Co in CH_3CN resulted in no evolution of gas. Reduction of the complexes by addition of "super hydride" (potassium tri-*sec*-butyl borohydride in THF) to **III**Br_2 and **III***Br_2 also resulted in the color change from orange to yellow-green. Upon addition of the acid the color

(28) (a) Lovecchio, F. V.; Gore, E. S.; Busch, D. H. *J. Am. Chem. Soc.* **1974**, *96*, 3109. (b) Busch, D. H. *Acc. Chem. Res.* **1978**, *11*, 392.

(29) Bard, A. J.; Faulkner, L. R. *Fundamentals and Applications of Electrochemical Methods*; Wiley: New York, 1980; p 431.

(30) Parker, V. D. *J. Am. Chem. Soc.* **1992**, *114*, 7458.

(31) Fakhr, A.; Mugnier, Y.; Laviron, E. *J. Organomet. Chem.* **1988**, *346*, C49.

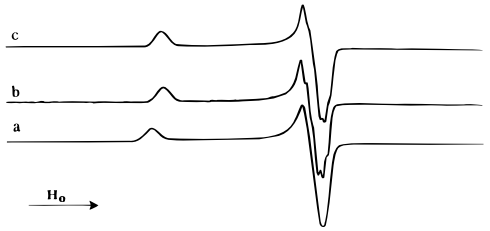

Figure 7. X-band EPR spectra obtained at 100 K from acetonitrile solutions of (a) **II***Br_2 ($g_\perp = 2.055$ and $g_{||} = 2.215$), (b) **III***Br_2 ($g_\perp = 2.059$ and $g_{||} = 2.208$), and (c) **IV***Br_2 ($g_\perp = 2.062$ and $g_{||} = 2.208$) after reaction with 1 equiv of cobaltocene.

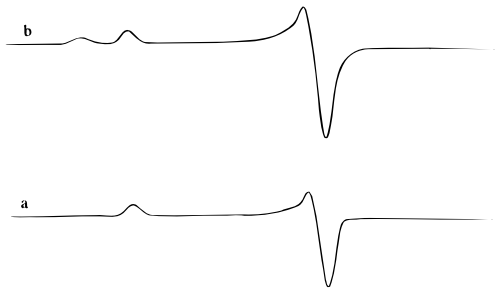

Figure 8. X-band EPR spectra obtained at 100 K from acetonitrile solution of iodide salts of (a) $[\mathbf{I}Me_2]^{2+}$ ($g_\perp = 2.067$ and $g_{||} = 2.245$) under N_2 atmosphere and (b) $[\mathbf{I}Me_2]^{2+}$ under CO atmosphere ($g_1 = 2.065$, $g_2 = 2.245$, and $g_3 = 2.297$), after reaction with 1 equiv of cobaltocene.

reverted to orange again, concurrently with evolution of hydrogen gas. In each case regeneration of the Ni^{II} complex was observed and confirms that the ligand remains associated to the nickel during reduction, consistent with the good binding ability of macrocycles.

EPR Studies. The X-band EPR spectra of the Ni^{I} macrocyclic complexes as prepared by cobaltocene reduction in acetonitrile solutions are presented in Figure 7. The *g* values of the observed axial signals are consistent with localization of the unpaired electron density on the $d_{x^2-y^2}$ orbital of the nickel, in a substantially square planar geometry. As shown in Figure 8a, an EPR signal similar to that for the macrocycles is obtained for the open chain $[\mathbf{I}Me_2]^+$, prepared by reduction of the iodide salt of the complex with 1 equiv of cobaltocene. Such axial EPR spectra are typical of several tetraazanickel(I) species reported by Gagne and Ingle, as well as by Busch et al.[28a,32]

Reaction of Ni^{I} Complexes with CO. While the cyclic voltammograms of the macrocyclic complexes under N_2 and CO atmospheres showed only minor differences, the open-chain iodide salt of $[\mathbf{I}Me_2]^{2+}$ showed a positive potential shift of the $Ni^{II/I}$ couple by 104 mV in the presence of CO, Figure 9. [Note: The minor shifts of the iodide oxidation peaks in the presence of CO were also observed in solutions of $[Bu_4N]I$.] The binding constant of CO to Ni^{I} was calculated from electrochemical data by a method similar to that used by Gagne and Ingle.[32] Since the electrochemical and chemical reversibility is a prerequisite for use of the $E_{1/2}$ shift for calculating binding constants, reversibility of the redox process was determined by cyclic voltammetry ($\Delta E_p = E_{pa} - E_{pc} = 59$ mV; E_p is independent of scan rate (ν) and $i_p \propto \nu$). The K_b value was calculated from the Nernst equation derived relationship for an electrochemical process that has reversible electron transfer followed by reversible ligand binding to the reduced species. That is, $\{e^{(\Delta E(nF/RT)} - 1\}^{-1} = \{K^{I} - K^{II}\}^{-1}\{[CO]\} + K^{II}\{K^{I} - K^{II}\}$, where K^{II} and K^{I} are the binding constants of CO to Ni^{II} and Ni^{I}, respectively.

(32) Gagne, R. R.; Ingle, M. *Inorg. Chem.* **1981**, *20*, 420.

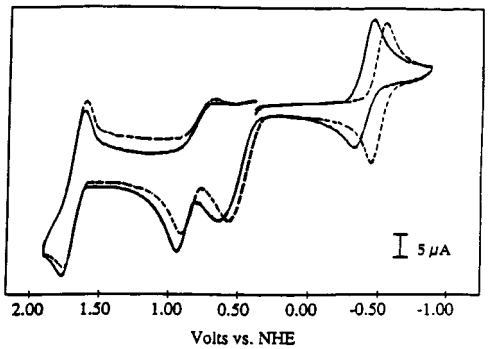

Figure 9. Cyclic voltammograms of the iodide salt of $[\mathbf{I}Me_2]^{2+}$ (2.5 mM) in CH_3CN under 1 atm of CO (—) and N_2 (- -). Experimental conditions are the same as in the caption of Figure 4.

Since CO does not bind to Ni^{II}, the equation simplifies to $e^{(\Delta E(nF/RT)} - 1 = K_b[CO]$. Using $\Delta E = 104$ mV, $K_b = 1.25 \times 10^4$ M^{-1}.[32,33] This value is comparable to the cyclam derivative macrocycle of Ni^{I} in DMF solution ($(1.7-4.5) \times 10^4$) and an order of magnitude higher than other macrocycles (2.7×10^3).[33]

A comparison of EPR spectra of the one-electron reduced iodide salt of $[\mathbf{I}Me_2]^{2+}$ in N_2 and CO atmospheres is shown in Figure 8. The spectrum of Ni^{I} shows an axial signal similar to the square planar macrocycles; under CO an additional signal, $g = 2.297$, is seen. The result may be interpreted as indicative of two EPR active species in solution, with similar $g_{||}$ (the 2.067 value) but different $g_\perp$ values. The additional signal is interesting in light of a previous study which found an isotropic EPR signal of a square planar Ni(I) complex (i.e. (3,6,10,13-tetraaza-1-bora-1,1-difluoro-4,5,11,12-tetramethyl-2,14-dioxacyclotetradeca-3,5,10,12-tetraenato)nickel(I)) which transformed to an axial signal in the presence of CO.[32] Should the interpretation expressed above, i.e., the EPR spectrum is actually that of two overlapping spectra due to the presence of an equilibrium in which a CO bound pentacoordinated Ni^{I} center is produced,[34] indeed be correct, we might expect the reduced macrocycles to be equally facile at binding CO. Indeed they are not, and the assignment of the geometry of the species in solution remains unresolved; however, other techniques, *vide infra*, support the CO binding.

Under 1 atm of CO gas, the low-temperature IR spectrum of the CH_3CN solution of $[\mathbf{I}Me_2]^+$ showed both free CO at 2141 cm^{-1} and an absorption at 2041 cm^{-1} which is assigned to Ni^{I}—CO. This band position is similar to that reported by Holm et al. for the CO adduct of the Ni^{I} derivative of a NS_3 tripodal ligand, 2026 cm^{-1}, and at the high end of the range reported for CO adducts of Ni^{I} derivatives of Gagne and Ingles' tetraazamacrocycle complex.[32,35] At room temperature additional bands appeared at 1960 and 2017 cm^{-1}, suggesting further reduction by CO and the presence of multiple Ni-bound carbonyls.[1]

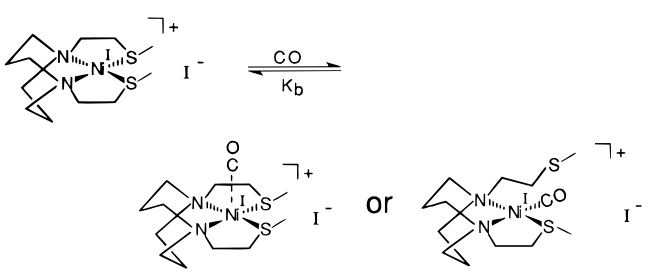

The CO-bound Ni^{I} species is also active in H_2 production in acidic solutions. Electrochemical studies similar to those

described above in CO-saturated solutions containing HBF_4 and $[\mathbf{I}Me_2]^{2+}$ with iodide counterions also showed evidence of EC′ behavior, i.e., an increase in the cathodic peak current at the expense of the anodic peak.

Summary and Comments

Primary conclusions arising from this study of macrocyclic complexes of nickel in the mixed donor environment of tertiary nitrogen/thioether sulfur ligation are as follows:

Synthesis and Structures. The *cis*-dithiolate complexes **I** and **I*** are effective in the template synthesis of macrocycles containing a relatively square planar N_2S_2 donor set whose capability to deform is limited to the dithioether portion of the macrocycle. In the absence of additional donor sites in the S to S linker, increasing linker size, C_2, C_3, and C_4, correlates with cavity enlargement (or Ni−S distance), S to S distance, and S−Ni−S angle.

Electrochemistry. In the absence of additional donor sites in the S to S linker the accessibility of Ni^{I} correlates linearly with macrocycle size and, presumably, with increased ligand flexibility, covering a range of −780 to −432 mV. The most accessible $Ni^{II/I}$ couple in the macrocyclic series is only 20 mV more negative than the open tetradentate ligand, $[\mathbf{I}Me_2]^{2+}$ ($Ni^{II/I}$ of **IV***Br_2, −432 mV vs NHE; $Ni^{II/I}$ of $[\mathbf{I}^*Me_2]^{2+}$, −412 mV). The decrease in the energy of the $d_{x^2-y^2}$ orbital of the nickel as the ring size increases, i.e., the in-plane ligand field strength decreases, brings about an easier reduction but a more difficult oxidation of Ni^{II} within the series, maintaining a ca. 2 V difference between Ni^{I} and Ni^{III}.

Comparison of Donors. While the N_2S_2 macrocycles based on diazacyclooctane derivatives readily achieve Ni^{I}, further reduction is at −2 V or beyond. Comparisons with tetraazamacrocycles of the same ring size (13- and 14-membered macrocycles) show a more difficult access to Ni^{I} (by ca. 0.7 V as compared to analogous N_2S_2 macrocycles), with no possibility of Ni^{0}.[28,34] In contrast phosphinothioether P_2S_2 complexes show $Ni^{II/I}$ in the range of −0.1 to −0.4 V, and $Ni^{I/0}$ is readily accessible in the −0.8 to −0.9 V range.[1] Notably the numbers quoted for P_2S_2Ni derive from open-chain complexes with the capability of deforming and accommodating a tetrahedral preference for Ni^{0}. Nevertheless, a major effect must be ascribed to the soft donor environment, provided by both phosphorus and thioether sulfur.

Evidence of Reactivity of Nickel(I). Although all the macrocyclic N_2S_2 complexes demonstrated accessibility of nickel(I), the formation of a relatively stable nickel(I) carbonyl adduct was only achieved in the open-chain analogue $[\mathbf{I}Me_2]^{+}$. While the CO adduct was indicated by IR and EPR spectra and cyclic voltammetry, it remains ill-defined as to geometrical structure and coordination number.

The ability of the Ni(I) complexes to reduce H^+ to H_2 was demonstrated by electrochemical measurements. In this case, the macrocycles are as, or possibly more, catalytically effective than the open-chain complex. A possible explanation of this observation may be based on electron count: while oxidative addition of H^+ to a 17-electron Ni^{I} complex to yield a 17-electron macrocyclic$-N_2S_2Ni^{III}-H^+$ is possible, addition of CO to yield a 19-electron macrocycle$-N_2S_2Ni^{I}(CO)^+$ adduct is not. The open-chain ligands with the possibility of CO replacement of a labile thioether might better accommodate adduct formation of a CO species.

Acknowledgment. Financial support from the National Science Foundation (Grant CHE 94-15901) for this work, Grant CHE-8513273 for the X-ray diffractometer and crystallographic computing system, and Grant CHE-8912763 for the EPR spectrometer along with contributions from the R. A. Welch Foundation are gratefully acknowledged. We thank Prof. Paul Lindahl's group for help with the EPR measurements. Insightful comments of a reviewer are sincerely appreciated.

Supporting Information Available: X-ray crystallographic files, in CIF format, are available on the Internet only. Access information is given on any current masthead page.

IC970526T

(33) Gagne, R. R.; Spiro, C. L. *J. Am. Chem. Soc.* **1980**, *102*, 1444.
(34) Hathaway, B. J.; Billing, D. E. *Coord. Chem. Rev.* **1970**, *5*, 143.
(35) Stavropoulos, P.; Carrié, M.; Muetterties, M. C.; Holm, R. H. *J. Am. Chem. Soc.* **1990**, *112*, 5385.